Coherent transport structures in magnetized plasmas. II. Numerical results

Coherent transport structures in magnetized plasmas. II. Numerical results

G. Di Giannatale, M. V. Falessi, D. Grasso, F. Pegoraro, and T. J. Schep

Citation: Physics of Plasmas **25**, 052307 (2018); doi: 10.1063/1.5020164
View online: https://doi.org/10.1063/1.5020164
View Table of Contents: http://aip.scitation.org/toc/php/25/5
Published by the American Institute of Physics

Coherent transport structures in magnetized plasmas. II. Numerical results

G. Di Giannatale,[1] M. V. Falessi,[2] D. Grasso,[3] F. Pegoraro,[4] and T. J. Schep[5]
[1]*IGI—CNR Corso Stati Uniti 4, 35127 Padova, Italy*
[2]*ENEA C.R. Frascati Via Enrico Fermi 45, 00146 Frascati, Italy and Dipartimento di Matematica e Fisica, Roma Tre University, Roma, Italy*
[3]*ISC—CNR and Politecnico di Torino Dipartimento Energia, C.so Duca degli Abruzzi 24, 10129 Torino, Italy*
[4]*Dipartimento di Fisica E. Fermi, Pisa University, largo Pontecorvo 3, 56127 Pisa, Italy*
[5]*Fluid Dynamics Laboratory, Department of Applied Physics, Eindhoven University of Technology, P. O. Box 513, 5600MB Eindhoven, The Netherlands*

(Received 20 December 2017; accepted 2 May 2018; published online 25 May 2018)

In a pair of linked articles (called Papers I and II, respectively), we apply the concept of Lagrangian Coherent Structures borrowed from the study of Dynamical Systems to chaotic magnetic field configurations in order to separate regions where field lines have different kinds of behavior. In the present article, Paper II, by means of a numerical procedure, we investigate the Lagrangian Coherent Structures in the case of a two-dimensional magnetic configuration with two island chains that are generated by magnetic reconnection and evolve nonlinearly in time. The comparison with previous results, obtained by assuming a fixed magnetic field configuration, allows us to explore the dependence of transport barriers on the particle velocity. *Published by AIP Publishing*. https://doi.org/10.1063/1.5020164

I. INTRODUCTION

In recent years, the concept of Lagrangian Coherent Structures (LCS) has been introduced by G. Haller in the context of transport processes in complex fluid flows, see Ref. 1. In an accompanying paper, here referred to as Paper I, Ref. 2, it was shown that such a concept can be usefully applied to the study of particle transport in a magnetized plasma when a chaotic magnetic field develops and the field line dynamics can be taken as a proxy for the particle dynamics. The rationale for such an assumption, which neglects, e.g., the effects of the electric and magnetic particle drifts, is to provide a simple, even if not exact, tool that depends on as few parameters as are meaningful, and that can be used in a general setting for the easy detection of the barriers to enhanced particle transport, as is the case considered here, by the growth of multiple island chains due to the onset of magnetic reconnection. In particular, in Paper I, it was recalled how to relate a magnetic field configuration, at a fixed physical time, to a Hamiltonian system where the role of "time" (Hamiltonian time) is taken by an appropriately chosen coordinate along the magnetic field lines. In the same article, after a brief summary of the so-called "lobe-dynamics" and of the related transport in a nonautonomous one-degree of freedom Hamiltonian system, the definition and the properties of the Lagrangian Coherent Structures (LCS) were recalled. In the case of a (Hamiltonian) time periodic configuration, i.e., of a configuration that is geometrically periodic in the direction of the magnetic field as is the case, e.g., of a toroidal configuration, the connection with the widely used Poincaré map approach was mentioned. Finally, in Paper I, the magnetic configuration that is used in the numerical simulations reported in the present paper was introduced and a simple generalization to the case where the LCS are defined so as to include the evolution of the magnetic configuration in time was discussed. The chosen magnetic configuration is based on the investigation presented in Refs. 3–5 of the nonlinear evolution of two chains of magnetic islands produced by magnetic reconnection.

In the present paper, the concepts introduced in Paper I are implemented numerically using a MATLAB tool developed by K. Onu, F. Huhn and G. Haller, see Ref. 6. First, the LCS are obtained by considering a snapshot at a fixed physical time of the evolving magnetic configuration by explicitly exploiting its periodicity in the "Hamiltonian" time [see Eq. (20) of Paper I]. Then, the same numerical procedure is used to include the evolution of the magnetic configuration in physical time. This allows us to explore the dependence of transport barriers on particle velocity.

This paper is organized as follows. In Sec. II, after recalling the main features of the magnetic configuration of interest, we introduce the adopted numerical computation scheme and briefly describe the precautions that have been used in its implementation. In Sec. III, we take the flux function in the magnetic Hamiltonian at a fixed physical time: we choose $t = 415$, i.e., before the onset of fully developed chaos. The corresponding LCS are then obtained numerically and compared to the structures in the Poincaré map. In Sec. IV, we consider the case of a magnetic field that evolves in physical time, i.e., the case where a charged particle moving in the plasma sees a time varying magnetic field during its motion and apply the simplified model described in Sec. VI B of Paper I. In this case, the corresponding dynamical system turns out not to be periodic in time and then we do not find it convenient to refer to the technique of the Poincaré map. The LCS are then obtained numerically for different particle streaming velocities along field lines with the aim of finding how do the LCS change with physical time, how they differ from those found at the fixed physical time, and, in addition, whether and how particle with different velocities can cross LCS calculated for

different particle velocities. Finally, the conclusions are presented.

II. SIMULATION SETTINGS AND NUMERICAL PROCEDURE

A. Magnetic configuration

As anticipated in Sec. VI of Paper I, in the present article, we study the LCS in a magnetic configuration of the form

$$\mathbf{B}_{eq} = B_0 \mathbf{e}_z + \nabla\psi(x,y,z,t) \times \mathbf{e}_z, \tag{1}$$

where $\psi(x,y,z,t)$ is the full magnetic flux function that includes the equilibrium and the time evolving perturbations. Periodicity is assumed in all three directions and the configuration is restricted to the domain $[-L_x, L_x] \times [-L_y, L_y] \times [-L_z, L_z]$ with $L_x = \pi, L_y = 2\pi, L_z = 16\pi$.

We recall that the expression of $\psi(x,y,z,t)$ that we use has been obtained by means of a numerical simulation in Ref. 3 (see also Refs. 4 and 5) by imposing a "double helicity" perturbation $\hat{\psi}_1(x,t)\cos(k_{1y}y + k_{1z}z) + \hat{\psi}_2(x,t)\cos(k_{2y}y + k_{2z}z)$, with $k_{iy} = m_i\pi/L_y$ and $k_{iz} = n_i\pi/L_z$, where $m_1 = m_2 = 1$ and $n_1 = 1$, $n_2 = 0$, at equilibrium of the form $\psi_{eq}(x) \propto \cos(x)$. The eigenfunctions of the initial perturbations $\hat{\psi}_1(x,0)$ and $\hat{\psi}_2(x,0)$ are localized functions on the resonant surfaces and the initial amplitude of $\hat{\psi}_1$ was chosen to be of the order of 10^{-4} and ten times bigger than that of $\hat{\psi}_2$. The resonant surfaces $x = x_i$ are defined by the condition $\mathbf{B}_{eq} \cdot \mathbf{k}_{1,2} = 0$ and, disregarding the mirror-doubling of the configuration caused by the assumed periodicity along x, are located at $x_1 = 0$ and $x_2 = 0.71$, respectively.

The field line equations are given by

$$\frac{dx}{dz} = -\frac{\partial\psi}{\partial y}, \quad \frac{dy}{dz} = \frac{\partial\psi}{\partial x}. \tag{2}$$

Perturbations with different "helicities" are required in order to make the Hamiltonian system described in Sec. II of Paper I non-integrable, i.e., to generate a chaotic magnetic configuration. In the following analysis, we will focus on the magnetic configuration at two different normalized (with respect to the Alfvén time) physical times, i.e., $t = 415$ and $t = 425$, in which chaos, initially developed only on a local scale (at $t = 415$), starts to spread on a global scale (at $t = 425$).

In order to minimize the computational effort, we simplify the Hamiltonian by imposing a threshold condition on the amplitude of the components of the Fourier expansion of $\psi(x,y,z,t)$ along x, y and z. The validity of this approximation has been verified and successfully tested in Ref. 4. The physical time evolution of $\psi(x,y,z,t)$ between $t = 415$ and $t = 425$ was found in Ref. 3 to be super-exponential and is modeled here by interpolating the coefficients of its Fourier expansion according to a quadratic exponential time law of the form

$$\exp(\gamma_{k_y,k_z}(t - t_1)^2) \quad \text{for } t > t_1 = 415, \tag{3}$$

where, on the basis of the numerical data, the coefficients γ_{k_y,k_z} are considered independent of the x-coordinate, and hence dependent only on the mode numbers k_y and k_z.

B. LCS computation scheme

In order to find the hyperbolic Lagrangian Coherent Structures, we use a MATLAB tool developed by Onu, Huhn, Huhn, and Haller, see Ref. 6. This tool detects the LCS on the basis of their characterization as the most repelling or attractive material lines advected within the fluid and relies on the definitions that we listed in Secs. V and V A of Paper I.

The key steps of the adopted procedure can be summarized by the following operations:

1. Defining a velocity field.
2. Computing the eigenvalues and eigenvectors of the Cauchy-Green strain tensor.
3. Filtering the data locating the most important LCS to characterize the system dynamics. Details of this filtering procedure will be given below.

The procedure starts with the integration of the Hamilton equations, Eq. (2), for the magnetic field lines. This enables us to calculate the flow map $\phi^z_{z_0}(x_0, y_0)$ [defined in Eq. (4) of Paper I] with z substituted for t and then to compute the Cauchy-Green strain tensor field, its eigenvalues and eigenvectors and the related Finite Time Lyapunov Exponent (FTLE) field, see Eq. (16) of Paper I, that gives the rate of separation in a finite time interval of nearby trajectories. The repelling LCS are then found following the conditions given in Sec. V A of Paper I. In particular, in lieu of Eq. (14), but following Ref. 6, we identify the strongest repelling curves as those passing through a local maximum of the FTLE field. The advantage of such a prescription is twofold: on the one hand, it significantly reduces the computing time and on the other hand it allows us to avoid the ambiguities related to the implementation of condition (14) of Paper I, that is $\boldsymbol{\xi}_{max} \cdot \nabla^2\lambda_{max} \cdot \boldsymbol{\xi}_{max} < 0$, on a discrete relatively sparse grid. Therefore, since we need a point from which to start the numerical integration of LCS, we take the largest local maxima of the FTLE field as starting points. In principle, we should solve for the curve defined by the condition $\boldsymbol{e}_0 = \boldsymbol{\xi}_{min}$ [Eq. (12) of Paper I], where we recall that $\boldsymbol{e}_0$ is the tangent vector to the material line and $\boldsymbol{\xi}_{min}$ the eigenvector of the Cauchy-Green strain tensor (corresponding to the smaller eigenvalue) starting from each local maximum. However, in chaotic systems, the FTLE field exhibits a huge number of local maxima and, in addition, the numerical evaluation of the matrix $\nabla\phi^z_{z_0}(x_0, y_0)$ produces a very discontinuous FTLE field. By integrating the above condition for each local maximum, we would find so many structures that they would confuse the physical information which we wish to extract. For these reasons, it is necessary to define a criterion to adopt in order to filter out the maxima that we consider not to be physically significant. It is assumed that the larger the area around a local maximum, the more significant the maximum will be. This criterion corresponds to take only those points that are absolute maxima of the FTLE field

within a predefined area. Therefore, we seek maxima of the FTLE field and then, if the distance between two maxima is smaller than the predefined maximization distance, we disregard the maximum with the lower value of the FTLE field. In other words, the number of LCS that we find depends on the value that we choose for the maximization distance in the code.

In order to clarify this criterion, let us suppose that two large maxima of the FTLE field are very close to each other, i.e., that their distance is smaller than the chosen maximization distance. In this case, only the largest maximum is used as a starting integration point. In general, this does not lead to a loss of physical information since if two maxima are strong and are very close to each other usually the LCS goes through both and thus the distinction between them is no longer necessary. However, it is also possible that two close maxima may give rise to different LCS: in this situation, we miss one LCS because we keep only one maximum. In the following, we will illustrate with a specific case how the maximization distance can affect the resulting LCS and the physical information that we can obtain on the system. In our simulations, we performed a series of tests to tune the value of the maximization distance in order to find the optimal value that allows us to characterize the behavior of the system avoiding to have to deal with too many structures. We used a resolution of 600 points in the x-direction and the number of points in the y-direction is set so as to have the same spatial resolution, i.e., $\Delta x = \Delta y$. Another critical parameter is the interval $z - z_0$, where z_0 is the initial Hamiltonian time, chosen in the computation of the Cauchy-Green tensor. In fact, if this interval is too small, we risk selecting structures that last for a too short z-interval: for example, we could also find LCS in a non-chaotic region, since two KAM tori with different velocities could be seen as divergent trajectories if the evolution time of the system is too small. On the other hand, if the integration interval is too long, the computational time grows and it may become very difficult to follow the eigenvectors of the Cauchy Green tensor. Moreover, as this interval increases, LCS tend to converge to the corresponding invariant manifolds which, as stated in Paper I, are characterized by a very convoluted structure. By carefully choosing this parameter, we are able to find structures with relatively simpler patterns which describe the coherent behavior of the system on a shorter interval. Additionally, if the z interval is too long, the LCS technique itself could be wrong because the LCS are computed using linear techniques [see Eq. (5) of Paper I]. In order to avoid the problems related to a possible bad choice of the z interval, the Cauchy-Green tensor has been computed by taking, in the periodic case, the numerical value of $\nabla\phi^{z}_{z_0}(x_0, y_0)$ every $8L_z = 4 \cdot 32\pi$. This means that the FTLE field is calculated after every 4 z-loops and that we can take, among the points that are maxima of the FTLE field at the end of the z-interval, those points that have after each 4 z-loops a value of the FTLE larger than the FTLE mean value (computed with the values taken at the grid points). Since, in our simulation, the interval $z - z_0$ is 16 loops, this corresponds to three checks. With this check, we ensure that we take as a starting point a point that repels particles at each time instant. In other words, we want to take a point that has a good repulsion property during the 16 loops of the simulation interval, although this does not necessarily imply that the repulsion properties can be extended to longer integration intervals.

Finally, special attention has been paid to the problem of noise arising from the use of a finite grid. This problem is enhanced in a chaotic system and is mitigated here, as mentioned before, by avoiding spurious maxima present only at the end of the $z - z_o$ interval and by filtering the LCS by means of the criterion described above.

III. THE *z*-PERIODIC CASE

In this section, we show the simulation results that we have obtained considering the Hamiltonian for the magnetic field line trajectories at a fixed physical time. We choose $t = 415$, i.e., before the onset of fully developed chaos.

A. Poincaré map

As stated above, once the physical time has been fixed, we can exploit the periodicity of the system along the z-direction and apply the Poincaré map technique by plotting the magnetic line intersection points in the x–y plane after each periodicity interval in z starting from a given initial value of z that defines the section chosen. This kind of plot is very useful since it provides information on the topological aspect of the magnetic field configuration, identifying the regions where the trajectories are regular and those where they are chaotic. Although the Poincaré map is fundamental to study a time periodic dynamical system, the LCS technique makes it possible to further partition the regions characterized by a chaotic behavior into sub-regions where trajectories have a qualitatively different behavior on the time intervals which characterize the LCS. Here, we focus on the section $z = 0$ and restrict the integration domain in the x-direction to the region in-between the two initial resonant surfaces where chaos develops first i.e., to $0 < x < 0.8$ and $-2\pi < y < 2\pi$. The corresponding plot for $z = 0$ is shown in Fig. 1. We note that a chaotic region exists between the two island chains that correspond to the initially imposed perturbations. However, regular regions survive in the chaotic sea: in particular, in Fig. 1, the regular region having y-periodicity $m = 3$ splits the domain into two sub-domains.

B. Lagrangian coherent structures

To find the LCS, it is first necessary to compute the field of the finite time Lyapunov exponents (see Secs. V and V B of Paper I) and then proceed with the trajectory integration starting from the points with the largest eigenvalue λ_{max}. The FTLE field is shown in Fig. 2. In the following, we restrict our search to repelling LCS, since we can exploit the space-time reflection symmetry $y \to -y$, $z \to -z$ introduced in Sec. VI A of Paper I in order to find the attractive LCS which are thus obtained by mirror reflection of the repelling ones with respect to the $y = 0$ axis.

In Fig. 3, the LCS that we have identified with the numerical procedure described in Sec. II B are overplotted

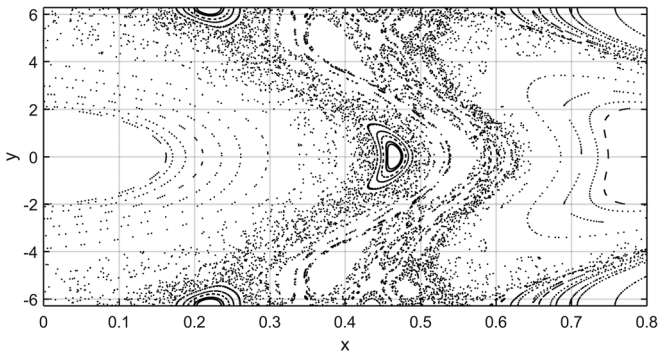

FIG. 1. Poincaré map at $z=0$ of the magnetic configuration taken at $t=415$. The map has been obtained evolving 150 initial conditions for $100L_z$. The initial conditions are uniformly distributed in the x-direction in the interval [0, 0.8] and have $y=-2\pi$. The white regions correspond to trajectories (i.e., to magnetic field lines) on regular surfaces in the extended x, y, z phase space. The larger ones at the edge of the domain are the magnetic islands corresponding to the initial perturbations, while the regular region, that is for $y=-2\pi$ located approximately between $x=0.35$ and $x=0.4$ corresponds to a chain having $m=3$ and splits the chaotic region into two sub-domains.

on the Poincaré map. The repelling (attractive) structures are drawn in red (blue). We recall that in the small amplitude linear phase, the two perturbations with different helicities evolve independently from each other and each of them induces a magnetic island chain around its resonant surface. If the Hamiltonian does not depend on z, these islands are delimited by the separatrices that are formed through the smooth connection of stable and unstable manifolds and that act as barriers. Here, the smooth connection between stable and unstable manifolds is broken since the magnetic configuration does not correspond to an autonomous dynamical system. The footprint of the breaking can be recognized in Fig. 3 close to the regular regions corresponding to the initial perturbations in the lobe-like shape that the LCS exhibit when approaching the edge of the domain. Since LCS mark the most repelling (attractive) material lines, they tend to follow the stable (unstable) manifolds that in non-autonomous cases continue to intersect the unstable (stable) manifolds. In Fig. 3, we mark with green arrows the most visible intersections that give rise to the lobes. In principle, the intersection should continue to generate a complex tangle, but our

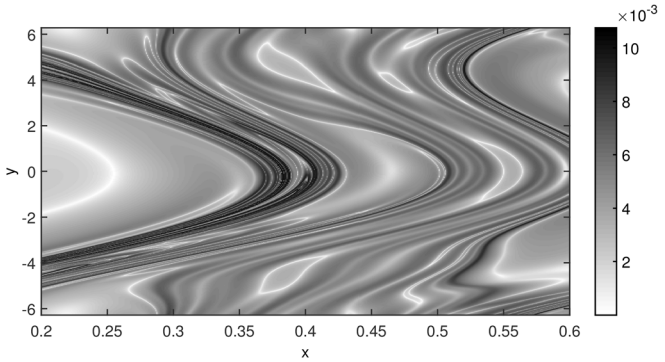

FIG. 2. FTLE field for the Hamiltonian at $t=415$, on the plane $z=0$. 500 points in x, and 7850 in y have been used so as to have the same resolution in both directions. The darker shading corresponds to larger values of the eigenvalue λ_{max} of the Cauchy-Green tensor.

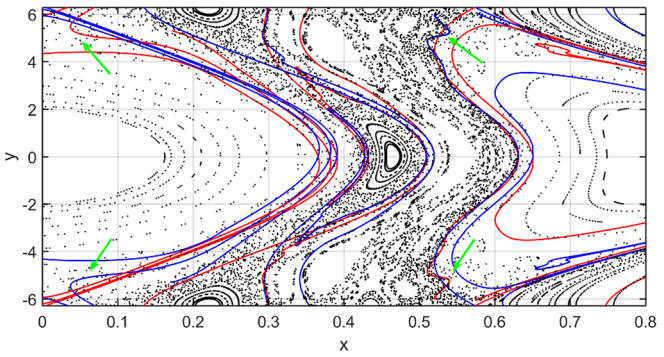

FIG. 3. Most important LCS overplotted on the Poincaré map at $z=0$ and $t=415$. The repelling (attractive) structures are drawn in red (blue). The green arrows indicate where the lobes and the tangle form.

numerical integration cannot follow the manifold oscillations indefinitely.

In order to test the robustness of these LCS as barriers, we performed a series of trajectory integrations of magnetic field lines considering an initial set of 20 initial conditions at a given position and letting these trajectories evolve for $80L_z$. All the initial conditions (i.c.) are localized into a radius of 0.003. Then, we plot their position in the x–y phase space at every crossing of the $z=0$ section on which we have calculated the LCS. Figures 4–6 confirm that the LCS that we have found act as strong barriers, since there is no flux through them on the considered time-span unless we consider regions with lobes and tangles. The location of the initial conditions is marked by an arrow in the figures. In the left panel of Fig. 4, by taking the initial conditions very close to the KAM surfaces that are still present in the chaotic sea that forms between the two main magnetic islands, we see how the LCS confine the evolution of these trajectories. On the contrary, in the right panel of Fig. 4, we set the initial conditions very close to the repelling LCS. In that region, lobes and tangles are expected, although they are not visible due to the small resolution: with the adopted resolution, we are able to follow the manifolds of the main islands, corresponding to the $m=1$ mode, but we cannot follow the manifolds of the smaller islands. In this region, according to the lobe dynamics briefly recalled in Sec. III of Paper I, particles can cross the barriers. In the remaining Figs. 5 and 6, the role of different LCS is again tested using the same technique.

Examining the plots of the LCS shown in the figures, we note that the repelling LCS, red lines in Fig. 3 (and similarly the attractive LCS, blue lines) appear not to be periodic in the y direction. Actually, this is a numerical effect related partly to the size of the integration grid and partly to the setting of the maximization distance described in Sec. II B. In fact, on decreasing the maximization distance used when selecting the FTLE maxima, additional LCS arise among which are those that match, at the edges of the y domain, the structures shown in the plots.

IV. THE *z*-NON PERIODIC CASE

In this section, we consider the case of a magnetic field that evolves in physical time. This implies that a charged

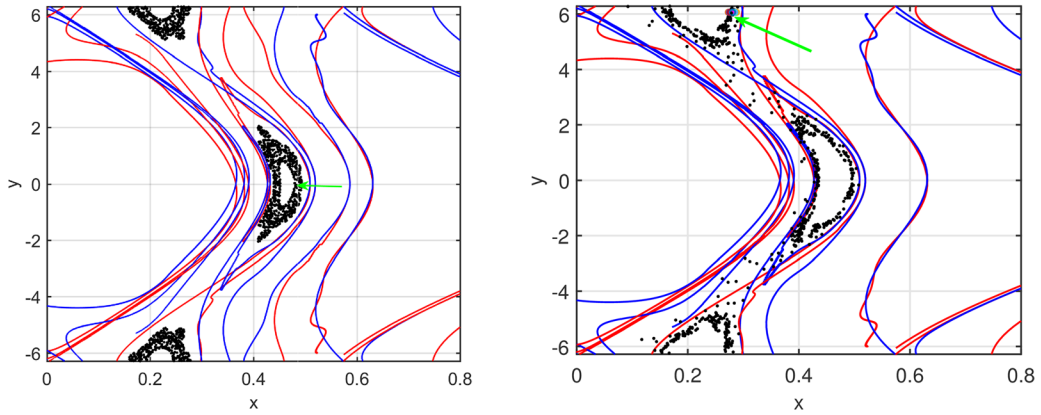

FIG. 4. LCS obtained using the Hamiltonian at $t = 415$. The left panel shows that the initial conditions taken in the regular region, bounded by hyperbolic LCS, remain confined inside this region. In the right panel, the initial conditions are very close to a repelling LCS and, therefore, some particles escape according to the lobe dynamics. The location of the initial conditions is marked by an arrow.

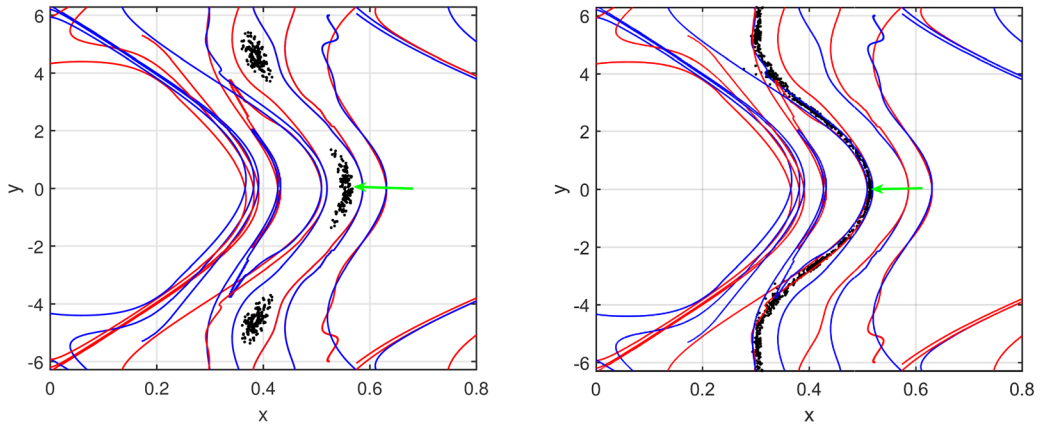

FIG. 5. LCS obtained for the Hamiltonian at $t = 415$. Both figures show how the drawn LCS act as barriers. Note that the trajectories belong to two different regions: in order to make the visualization easier in the right frame, we have deleted the LCS that confine the set of initial conditions to the left frame. The location of the initial conditions is marked by an arrow.

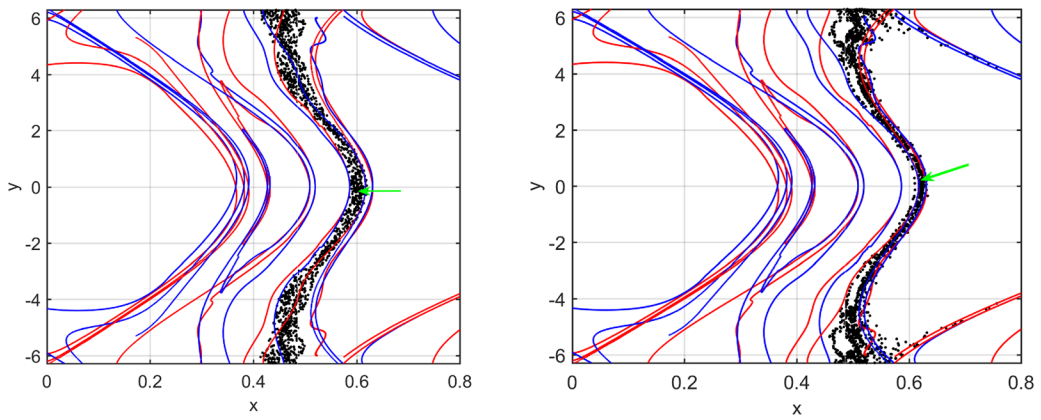

FIG. 6. LCS obtained using the Hamiltonian at $t = 415$. Both figures show how the drawn LCS act as barriers. Note that the figure in the right frame has been obtained by reducing the value of the maximization distance with respect to that in the left frame. A new LCS arises and it splits the chaotic domain in the left frame into two sub-domains. Both domains are chaotic, but they cannot communicate. This underlines the fact that if we take a smaller value of the maximization distance, we can find additional transport barriers. The location of the initial conditions is marked by an arrow.

particle moving in the plasma sees a time varying magnetic field during its motion. The main questions that we intend to address are: how do the LCS change with physical time, how different are the new LCS from those found at the fixed physical time, and finally if and how particles can cross LCS constructed for particles with a different velocity.

We examined a time interval extending over 10 normalized units from $t_1 = 415$ to $t_2 = 425$. Chaos has developed during this time interval as shown by the Poincaré map in Fig. 7 for $t = 425$ i.e., at the end of the interval.

We adopt the simplified model, where particles move with a constant velocity V along the z-direction only,

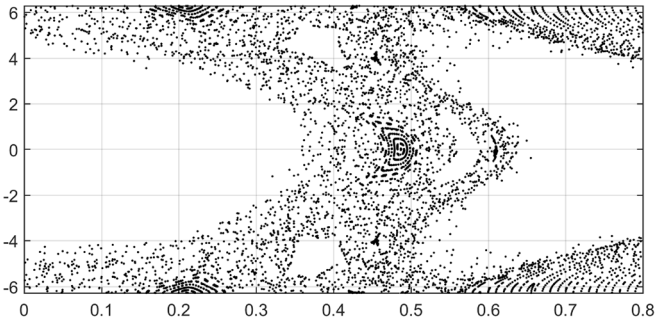

FIG. 7. Poincaré map at $z=0$ and $t=425$.

described in Sec. VI B of Paper I. Then, the new Hamiltonian is given by the modified flux function

$$\psi_{\mathcal{V}}(x,y,z) \equiv \psi(x,y,z,t=(z-z_o)/V). \tag{4}$$

See Eq. (20) of Paper I, where the physical time dependence is chosen according to Eq. (3) and the dependence of $\psi_{\mathcal{V}}$ on the z variable combines the spatial and time dependence of the magnetic configuration, as seen by a particle streaming with velocity V along a field line. We use this Hamiltonian to calculate LCS for different values of velocity V. Note that although simulations with different values of V have been performed, unless specified, the LCS shown in the figures are those for particles with velocity $V=1000$. With this value, the particles perform 10 z-loops in one time interval. This is a compromise between having a magnetic field that does not evolve too fast during the motion of particles and being able to show the dependence of the LCS on the velocity V and investigate whether or not the LCS computed for a given velocity V act as a barrier also for particles with different velocities. In the following, we will focus on particles with a positive velocity. We stress that in this model, the z periodic case corresponds to the assumption that the particles move with infinite speed, and thus experience a fixed magnetic configuration.

First, we note that if we keep the number of z-loops fixed the LCS that are found with increasing velocity turn out to be similar to those found in the periodic case, as expected when the particles' travelling time is much shorter than the time over which the magnetic field changes.

Thus, in order to show in a more evident way the LCS in a time evolving magnetic configuration as seen by a particle with velocity V, we integrate the Hamilton equations (2) with the flux function $\psi_{\mathcal{V}}$ in Eq. (4) over fixed time intervals i.e., in terms of the variable t instead of z using the relationship introduced below, that is $t=(z-z_0))/V$. The change of variable from z to t and the definition of the time intervals need to be performed differently when computing repelling and when computing attractive LCS.

A. Repelling LCS

For the calculation of repelling LCS, we relate t to z in the Hamilton equations such that $t-t_0=(z-z_o)/V$.

First, we show how LCS evolve in time i.e., we calculate LCS at time $t=\bar{t}_0$ and position z_0, then, we "follow" the structures computing them at time $\bar{t}_1$ and position z_1, at time $\bar{t}_2$ and position z_2, and so on. To do this, we set $V=1000$ and choose the initial particle position, i.e., $z_0=0$, for all particles. Due to the long computational time and the fact that the adopted method uses linear techniques, we choose to evaluate the LCS integrating the initial conditions for a maximum of 20 z-loops. For a velocity $V=1000$, 20 z-loops correspond approximately to $\Delta t=2$. In order to investigate how the time-dependent magnetic field can affect the evolution of the LCS, we evaluate the structures at different times $\bar{t}_n$, starting from $\bar{t}_0=415$, since the time-independent analysis has been carried out at $t_1=415$. We divide the interval $[\bar{t}_0=415, \bar{t}_0+\Delta t=417]$ into sub-intervals of duration $\delta t=0.1$. We update the Hamiltonian according to Eq. (4), where, however, we express z in terms of t (instead of t in terms of z) as discussed before in Sec. IV A, and then integrating after each δt for the time interval $\Delta t=2$ we obtain a set of LCS at times $\bar{t}_n=415, 415.1, 415.2$ up to 417. This allows us to determine how the LCS computed at $\bar{t}_0=415$ evolve in time. For the sake of clearness, since the integration duration interval is fixed to $\Delta t=2$, in the figure captions, only the time at which the LCS structure is calculated will be indicated and not the starting and final integration time used to obtain them.

Using these LCS data, we show how particles initially separated by a repelling LCS evolve in such a way that they remain apart and do not cross the LCS itself as they evolve in time.

Particles with different velocities have different trajectories, and therefore different LCS. We investigate the dependence of these structures with respect to V. As can be seen from the simulation results, LCS act locally, i.e., an exponential departure from a repelling LCS is not observed. Initial conditions feel the "repulsion" of a repelling LCS only when they are very close to it. Due to this local influence, two sets of i.c. divided by a repelling LCS evolve initially in such a way so as to maximize the distance from the repelling LCS, e.g., see Fig. 10. After this first stage, they have different evolution.

B. Attractive LCS

For the attractive LCS, we relate t to z in the Hamilton equations such that $t-t_{end}=(z-z_{end})/V$. As explained in Paper I, we compute the attractive LCS as repelling LCS of the backward time dynamics. We show how attractive structures affect particle dynamics and how essential they are in order to understand the transport features of the system. Looking only at the repelling LCS, we can only have a partial understanding of the dynamics, e.g., we are able to say that two sets of i.c. divided from a repelling structure evolve in order to stay apart, but if we also want to know how "fast" are the mixing phenomena for those i.c., we need to calculate the attracting LCS. Following these considerations, we think that attractive LCS give a more intuitive description of the dynamics. In particular, they offer an understanding about how a big set of i.c. evolves. We remember that when we evolve the system from $t_{end}=417$ to $t_{end}-\Delta t=415$ to compute the attracting LCS, the structures are those corresponding to $t_{end}=417$ and they describe the behavior of

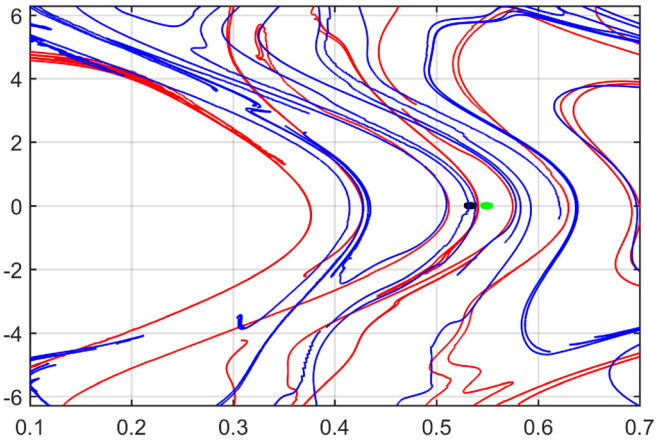

FIG. 8. Location at $t = 415$ of the initial conditions that will be followed in the next figures. They are located on the two sides of a repelling LCS (red), in a circle of radius equal to 0.003 at (0.53, 0) (black) and at (0.55, 0) (green). The difference with respect to Fig. 3 is due to the fact that, in this section, the time dependence of the magnetic field is taken into account, and thus particles, during their motion, do not see a time-frozen field (like in the time independent case) but an evolving magnetic field.

particles at time $t = 415$. Also, for attractive LCS, to simplify the notation, in the figure captions, we will not indicate the initial and final integration times. Finally, we remark that attractive LCS also act as transport barriers. In the Numerical results section, we exploit this fact to show that particles with velocity V_1 can cross barriers obtained considering a different velocity V_2.

C. Numerical results

In Fig. 8, two sets, each with 75 initial conditions, (marked green and black) are located on the two sides of a repelling LCS. The i.c. in each set are inside a circle with the radius equal to 0.003. In Figs. 9–11, the evolution of these two sets is shown. During the first part of the evolution, Fig. 9, the particles move away from the nearby repelling LCS positioning themselves in such a way so as to maximize their stretching in the perpendicular direction with respect to the LCS. In this phase, the two sets of i.c. behave similarly. In the left panel of Fig. 10, it appears clearly that after only $\Delta t = 0.5$, the two sets of conditions have evolved obeying two different kinds of dynamics. Few time intervals are sufficient to recognize the chaotic dynamics of the black initial conditions: their distribution becomes more stretched and convoluted than that of the green conditions since they are influenced by the presence of a nearby attractive structure. This tendency is more and more evident with increasing time, as shown in Figs. 10 and 11.

These results make the role of repelling and attractive LCS evident when describing the evolution of the system. In particular, the presence of a nearby attractive LCS seems to give rise to faster mixing phenomena. In Figs. 12 and 13, we show how particles feel the presence of attractive LCS. Both figures show how particles with $V = 1000$ behave in accordance with the LCS. This is due to the fact that the LCS have also been constructed for particles having $V = 1000$. The difference between the two figures is due to the spatial distribution of the i.c.

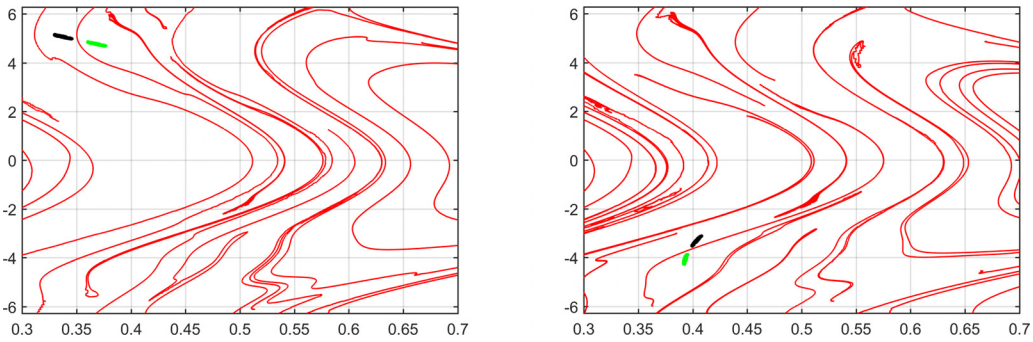

FIG. 9. Evolution of the initial conditions of Fig. 8 at $t = 415.1$ (left panel) and $t = 415.2$ (right panel) overplotted on the corresponding repelling LCS (red).

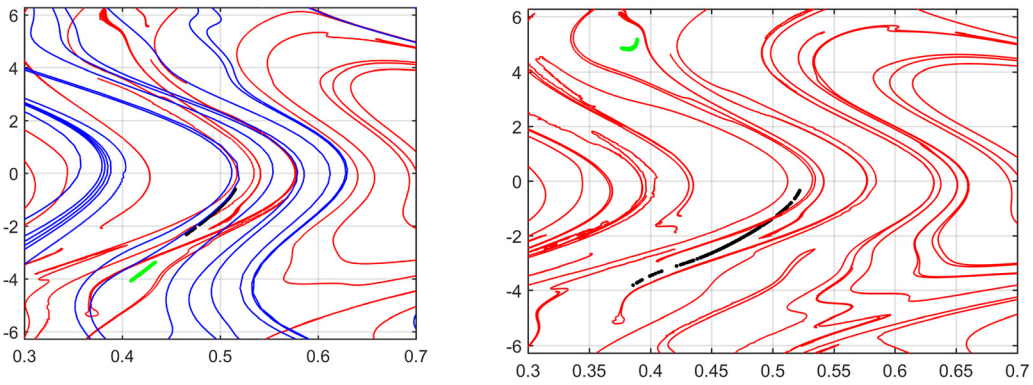

FIG. 10. Evolution of the initial conditions of Fig. 8 at $t = 415.5$ (left panel) and $t = 416$ (right panel) overplotted on the corresponding repelling LCS (red). In the left panel, the attracting LCS (blue curves) are also plotted in order to show that the particles arrange themselves along these curves.

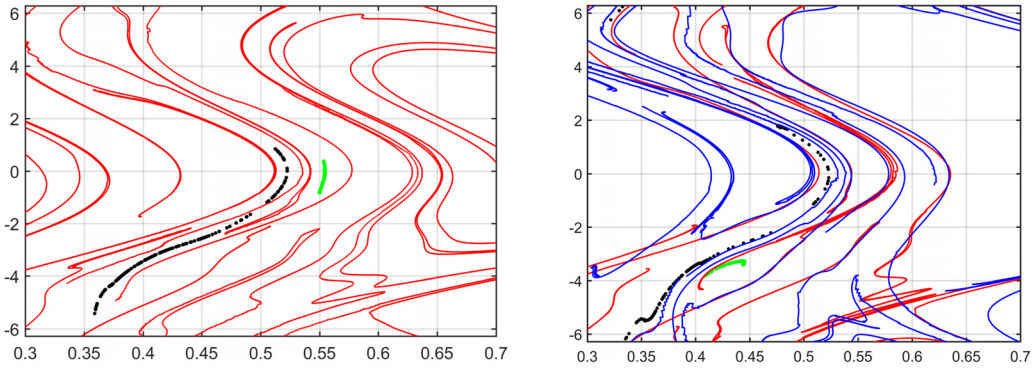

FIG. 11. Evolution of the initial conditions of Fig. 8 at $t = 416.5$ (left panel) and $t = 417$ (right panel) overplotted on the corresponding LCS. In the right panel, the attracting LCS (blue curves) are also plotted in order to show that the particles arrange themselves along these curves.

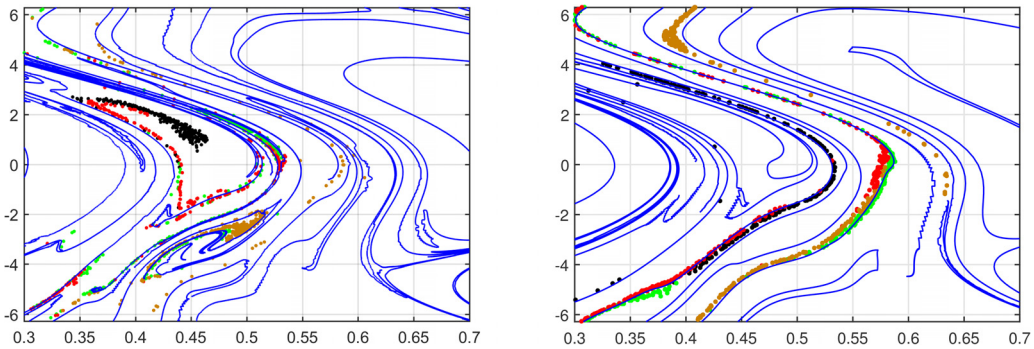

FIG. 12. Evolution of particles overplotted on the corresponding attractive LCS. For both figures, there are 500 i.c. for each color spread in the interval defined by $x = [0.5, 0.55]$, $y = [0, -1]$ for the black particles, $x = [0.5, 0.55]$, $y = [-1, -2]$ for the red ones, $x = [0.55, 0.6]$, $y = [0, -1]$ for the green ones and $x = [0.55, 0.6]$, $y = [-1, -2]$ for the brown ones. Particles in left panel start at time $t = 416$ and the figure shows their position at $t = 418$. Particles in the right panel start at $t = 418$ and in the plot their position at $t = 419$ is shown.

In Fig. 13, although the i.c. are very localized, due to the presence of LCS, they stretch in order to arrange themselves along the nearest attractive LCS and each color set remains well separated from the other ones because they are initially divided by repelling and attracting LCS (see the right panel of Fig. 13).

On the contrary, in Fig. 12, we use spatially spread initial conditions covering the region $x = [0.5, 0.6]$, $y = [0, -2]$. There are 500 i.c. for each color: black particles in the region defined by $x = [0.5, 0.55]$ and $y = [0, -1]$; red particles in the region defined by $x = [0.5, 0.55]$ and $y = [-1, -2]$; green particles in the region defined by $x = [0.55, 0.6]$ and $y = [0, -1]$; and brown particles in the region defined by $x = [0.55, 0.6]$ and $y = [-1, -2]$. The left panel shows the positions of the particles, starting at time $t = 416$ and at time $t = 418$. The blue lines are the attractive LCS computed starting from $t = 418$ to $t = 416$. The right panel shows the positions of particles, starting at time $t = 418$ and at time $t = 419$. The blue lines are the attractive LCS computed starting from $t = 419$ to $t = 418$. The interesting behavior is that although

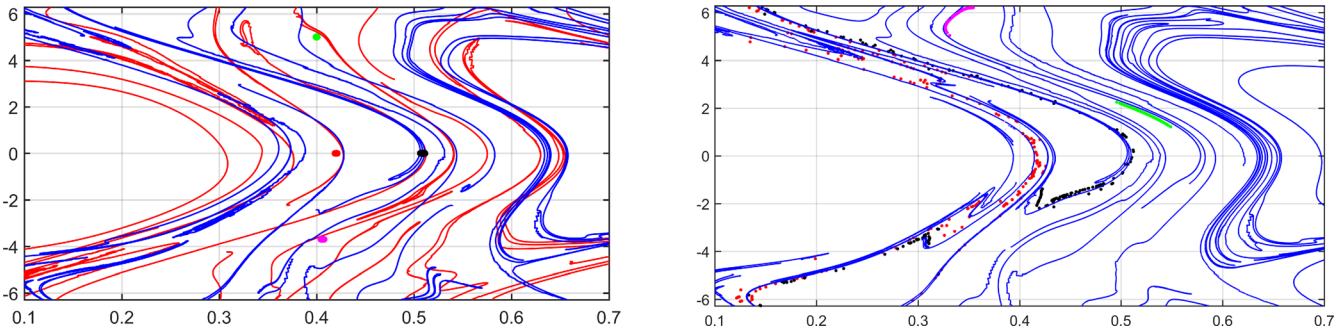

FIG. 13. In this and the following figure, the comparison between different velocities is shown. Here is the evolution of particles with $V = 1000$. In the left frame, the initial conditions at time $t = 415$ are shown. Each color corresponds to 300 i.c.: the green ones are located at $x = [0.398, 0.401]$, $y = [4.97, 5.02]$, the red ones are located at $x = [0.418, 0.421]$, $y = [-0.02, 0.02]$, the black ones are located at $x = [0.507, 0.511]$, $y = [-0.023, 0.023]$ and the magenta ones are located at $x = [0.404, 0.408]$, $y = [-3.71, -3.68]$. On the right panel, their evolution at time $t = 417$ is overplotted on the corresponding attractive LCS.

the i.c. cover a wide region, they evolve in such a way so as to position themselves according to the attractive LCS. This is the reason why often LCS are referred to as the "skeleton" of the dynamics. This behavior is even more evident in the right panel of Fig. 12, where we present the results obtained for a shorter integration time interval ($\Delta t = 1$). In general, better results are obtained if shorter time intervals are used and this could be due to two reasons: the first one is linked to the fact that we use a linear approximation in deriving the Cauchy-Green tensor and the second one is a consequence of the fact that when the time interval increases, the structures become much more convoluted so that, in order to evaluate them in a suitable way, it is necessary to have a higher spatial resolution.

Finally, we compare the LCS calculated for particles with $V = 1000$ with the dynamics of particles with different velocities. Taking the same initial conditions depicted in Fig. 13, but this time with $V = 200$, we find, as shown in Fig. 14, that they behave differently with respect to the LCS calculated for $V = 1000$. In the left panel of Fig. 14, we show the initial position of the particles and the repelling LCS computed integrating for $\Delta t = 10$ assuming $V = 200$ and, in the right panel, the new position of particles after $\Delta t = 10$ with the attractive LCS computed with $V = 1000$ (to show how particles with $V = 200$ can cross barriers obtained with velocity $V = 1000$) and $\Delta t = 2$. The choice $\Delta t = 10$ has been made in order to have the same number of z-loops (about 10) of the case $V = 1000$ shown in Fig. 13 and compare the results. While in Fig. 13, the particles arrange themselves along the attractive LCS; in Fig. 14, on the contrary, such a relation between the attractive LCS (computed for particles with $V = 1000$) and the position of the particles (having $V = 200$) is not present. In particular, although the particle positions appear qualitatively similar to those in Fig. 13, black particles with $V = 200$ are shifted with respect to black particles having $V = 1000$. This is due to the fact that the magnetic field configuration at time $t = 425$ (see the Poincarè plot in Fig. 7) has the $m = 2$ island chain shifted to the right with respect to its position at $t = 415$ (see the Poincarè plot in Fig. 1): at time $t = 425$, the $m = 2$ island has the O-point at $y = 0$ and $x = 0.485$, instead at $t = 415$, the corresponding O-point is at $y = 0$ and $x = 0.46$. The same explanation also holds for some red particles that seem to be able to cross through a region that at time $t = 415$ is regular. Moreover, we can also see that red particles with $V = 200$ behave "more chaotically" than red particles in Fig. 13. This is probably due to the fact that, as can be seen in the left panel of Fig. 14, red i.c. are divided by two repelling LCS (red curves). Finally, the magenta particles also find themselves in a different region with respect to the case $V = 1000$ (although their behavior in the two cases is quite similar).

As a general remark on the results shown in this section, we comment that the presence of several LCS makes it difficult to identify the ones that can be expected to be most relevant to the description of the particle transport. This complexity of the LCS structure is intrinsically related to the non-dissipative reconnection process that induces increasingly small spatial scales as it evolves in time.

V. CONCLUSIONS

Lagrangian Coherent Structures have been shown to provide a very convenient tool to identify in a compact and easily visualizable way the main features of the dynamics of the physical system under consideration. Clearly, with large computers and long integration times, one can recover all the needed information just following the individual particle trajectories of a large number of initial conditions. However, LCS do not simply provide the salient features that can be extracted from such large scale integrations but provide a framework and a language to be used in characterizing the evolution of such features in time.

In this and in the accompanying paper (Paper I), we have applied the LCS tool to study the dynamics of charged particles in a magnetized plasma in the presence of a time evolving reconnection instability. The LCS method is generally applicable without approximations by referring to the full particle dynamics in $3D$ coordinate space and by employing e.g., the exact particle Hamiltonian in time varying electromagnetic fields. Here, however, we have made use of two important simplifications with the aim of illustrating the method rather than of obtaining exact results to be applied to a specific fusion experiment configuration. In the first model we have used the magnetic field lines in a slab configuration at a given physical instant of time as a proxy for the particle trajectories. In the second model, we have

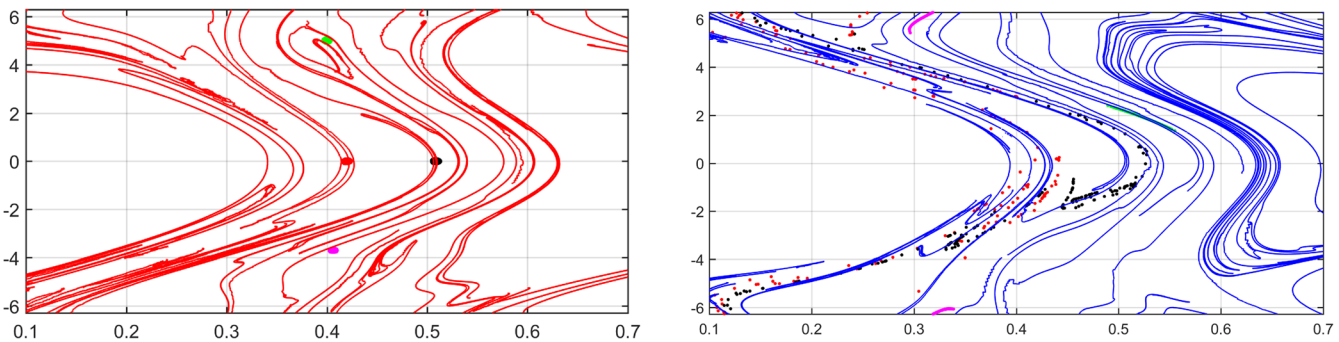

FIG. 14. Left panel: initial position at time $t = 415$ of particles and repelling LCS computed for particles with $V = 200$ with the integration path $\Delta z = 19.9$ z-loops (corresponding to $\Delta t = 10$). The location of initial conditions is the same as Fig. 13. Right panel: new position of particles having $V = 200$ at time $t = 425$ with overplotted on the attracting LCS computed with $V = 1000$ and the same integration path $\Delta z = 19.9$ z-loops, which corresponds to $\Delta t = 2$ and $t = 417$.

introduced an elementary procedure in order to account in an approximate way of the fact that the magnetic configuration evolves in time during the particle motion. In both cases, we have been confronted with a 2*D* phase space, much simpler than the full 6*D* phase space that would be required when solving the full particle dynamics, or the 4-dimensional phase space that is used in a time dependent guiding-center orbit description as in Ref. 7. Clearly, this major simplification has been made possible by the fact that in the adopted configuration, a strong and almost uniform magnetic field is present that, in a toroidal laboratory configuration, would correspond to the toroidal field. The first model has allowed us to relate the structures that govern the global dynamics of the particles to the evolution of the magnetic islands due to the development of magnetic reconnection. The second model has allowed us to show, even if in a rather schematic way, that these structures depend on the particle velocity (i.e., indirectly on the particle energy). We conclude by reiterating that the methods developed in these two papers can be extended to more refined dynamical descriptions, such as, e.g., a description based on the particle gyrokinetic approximation.

ACKNOWLEDGMENTS

G.D.G. and D.G. thank Dario Borgogno for fruitful discussions. Computational resources were provided by hpc@polito, which is a project of Academic Computing within the Department of Control and Computer Engineering at the Politecnico di Torino (http://www.hpc.polito.it).

[1]G. Haller and G. Yuan, Phys. D: Nonlinear Phenom. **147**, 352 (2000).
[2]G. Di Giannatale, M. Falessi, D. Grasso, F. Pegoraro, and T. Schep, Phys. Plasmas **25**, 052306 (2018).
[3]D. Borgogno, D. Grasso, F. Porcelli, F. Califano, F. Pegoraro, and D. Farina, Phys. Plasmas **12**, 032309 (2005).
[4]D. Borgogno, D. Grasso, F. Pegoraro, and T. Schep, Phys. Plasmas **15**, 102308 (2008).
[5]D. Borgogno, D. Grasso, F. Pegoraro, and T. Schep, Phys. Plasmas **18**, 102307 (2011).
[6]K. Onu, F. Huhn, and G. Haller, J. Comput. Sci. **7**, 26 (2015).
[7]H. Wobig and D. Pfirsch, Plasma Phys. Controlled Fusion **43**, A695 (2001).